Single-Pixel Remote Sensing

Jianwei Ma

***Abstract*—In this letter, we apply a new sampling theory named compressed sensing (CS) for aerospace remote sensing to reduce data acquisition and imaging cost. We can only record directly single or multiple pixels while need not the use of additional compression step to improve the problems of power consumption, data storage, and transmission, without degrading spatial resolution and quality of pictures. The CS remote sensing includes two steps: encoding imaging and decoding recovery. A noiselet-transform-based single-pixel imaging and a random Fourier-sampling-based multipixel imaging are alternatively used for encoding, and an iterative curvelet thresholding method is used for decoding. The new sensing mechanism shifts onboard imaging cost to offline decoding recovery. It would lead to new instruments with less storage space, less power consumption, and smaller size than currently used charged coupled device cameras, which would match effective needs particularly for probes sent very far away. Numerical experiments on potential applications for Chinese Chang'e-1 lunar probe are presented.**

***Index Terms*—Aerospace remote sensing, compressed sensing (CS)/compressive sampling, curvelets, lunar probe, single-pixel imaging, sparse recovery.**

I. Introduction

REMOTE sensing by satellites and aerospace probes is an important approach for deep-space exploration. This involves two basic stages: imaging by a digital camera and transmitting the data back to Earth. Based on conventional imaging principle, millions of pixels have to be stored momentarily when we take a picture using a megapixel camera. More pixels are often needed for higher resolution. However, they require a huge storage space in memory or hard disk. In order to reduce the storage, an immediate data compression takes place inside the camera by an embedded tiny microprocessor performing a discrete cosine transform for JPEG format or a discrete wavelet transform for JPEG 2000 format. For instance, a 6.1-megapixel digital camera senses 6.1×10^6 samples to construct an image, but in fact, a compressed image with average size smaller than 1 MB is saved in memory. Discarding lots of small transform coefficients and reconstructing retained significant coefficients to compressed pictures, in fact, we only save very limited numbers for later processing. The procedure is extremely wasteful for massive data acquisitions and batteries, particularly for large-scale aerospace remote sensing. On the other hand, in order to transmit the data collected by satellites back to Earth, we have to achieve huge compression ratios (CRs), which introduces inevitable distortions and mosaic artifacts. Our dream is whether we can only record directly one or very limited pixels (without the use of additional compression step) to improve the problems of storage, power consumption, and transmission, without degrading spatial resolutions and qualities.

A technique called compressed sensing (CS) or compressive sampling was recently proposed by Candès *et al.* [1]–[3] and Donoho [4], which makes it possible to solve these problems. The CS is an emerging and exciting field of research, which offers a novel sampling theorem for data acquisition by dealing with the combination of sensing and compression. The CS theorem says that a compressible unknown signal can be recovered from highly incomplete sets of linear measurements by a specially designed nonlinear recovery algorithm. Unlike traditional measurements that have to satisfy Shannon/Nyquist sampling theorem, i.e., the sampling rate must be at least twice the maximum frequency of signals, the CS measurement only obeys sub-Shannon rate without the limitation of Fourier bandwidth. The number of necessary measurements is far fewer than those required by traditional methods. The CS might have an important impact for design of measurement devices in various engineering fields, particularly where measurements are limited by physical constraints or data acquisition is expensive. A few potential applications of CS theorem have been made [5], [6], [9]–[11], [13] for compressive imaging, wireless sensing, optical architecture, etc.

In this letter, we apply the CS for aerospace remote sensing. The CS-based remote sensing includes two stages: onboard encoding imaging and offline decoding recovery. The encoding imaging can be implemented by single or multiple pixels/sensors, so that it could save the sensors, which not only saves the cost of sensors but also reduces the size and weight of onboard imaging instruments. Due to without the use of immediate compression step, the CS remote sensing can save power consumption. The encoding captures the compressed form of a scene directly, which is important to save the burden and cost when the data are transmitted back to Earth from satellites. These properties would match effective needs, particularly for probes sent very far away. Another potential advantage of CS imaging is that it can work much more easily for low light and outside the visible light spectrum due to the use of only one photon detector, so that it is potential for night-vision and infrared imaging [9]. In decoding step, we apply an iterative curvelet thresholding method for recovery. The CS remote sensing essentially shifts the online imaging cost to the computational cost of offline recovery.

In the following sections, we describe the encoding and decoding of the CS remote sensing, respectively.

II. Onboard Encoding: Compressed Imaging

Mathematically, we handle a fundamental problem of recovering a finite signal x from a small set of measurements y. Let

Manuscript received July 27, 2008; revised October 1, 2008 and November 3, 2008. This work was supported in part by the National Science Foundation of China under Grants 40704019 and 40674061, by the Tsinghua Basic Research Fund (JC2007030), and by the PetroChina Innovation Fund (060511-1-1).

The author is with the School of Aerospace, Tsinghua University, Beijing 100084, China (e-mail: jma@tsinghua.edu.cn).

Color versions of one or more of the figures in this paper are available online at http://ieeexplore.ieee.org.

Digital Object Identifier 10.1109/LGRS.2008.2010959

Φ be a $K \times N$ CS measurement matrix. Here, $K \ll N$, i.e., the rows of matrix are much fewer than the columns of matrix. In practice, Φ might denote an optical imaging lens. The encoding can be described as [2]

$$y = \Phi x + \epsilon \tag{1}$$

where ϵ denotes possible measurement errors or noises. The K denotes the number of measurements, and N denotes the dimension of the signal x. It seems hopeless to solve the ill-posed underdetermined linear systems of equations since the number of equations is much smaller than the number of unknown variables. Such problems are common in a variety of cases, e.g., the number of sensors is limited or the measurements are extremely expensive and time consuming. However, most time, x is compressible by a sparse transform Ψ; thus, we have $y = \Phi\Psi\vartheta + \epsilon$. If the measurement matrix Φ is noiselike incoherent in the Ψ domain, i.e., $\Phi\Psi$ satisfies a sufficient condition named restricted isometry property [1], [5], the CS told us that the sparse coefficients ϑ can be accurately recovered by solving a sparsity-promoting l_1-minimization or basis pursuit [2]

$$\min_{\vartheta} \|y - \Phi\Psi\vartheta\|_2^2 + \lambda\|\vartheta\|_{l_1} \qquad x = \Psi\vartheta. \tag{2}$$

The first term is a penalty that represents closeness of the solution to observed scenes. The second term is a regularization that represents *a priori* sparse information of original scenes. λ is a regularization parameter that can be tuned. Here, we simply use $\lambda = 1$. The best choice for λ depends on the variance of the noise and problem size parameters.

The CS, in fact, extends traditional pixel sensing to linear projection sensing, i.e., to measure inner products between the scene and a set of test functions. If Φ is an identity matrix or its sensing waveform is spikelike Dirac delta functions, the method degenerates to traditional space-domain measurements obeying Nyquist rate. If the waveforms are sinusoids, y is a vector of Fourier measurements. The choice of Φ and Ψ is critical for CS. In general, we can hire a measurement matrix by the following rules.

1) Universality: Φ should be noiselike incoherent/uncorrelated with a variety of sparse transform bases Ψ for natural scenes. That is to say, Φ and Ψ are as different as possible; thus, sampling waveforms have dense representation in Ψ.
2) Optimal performance: For a good Φ, the minimal number of necessary measurements to obtain a super-resolution result should be close to the theoretical bound $\mathcal{O}(S \log N)$ for an S-sparse N-dimension signal. The S-sparse means an object with at most S nonzero entries in a transform domain. The greater incoherence between Φ and Ψ, the smaller number of measurements is needed.
3) Fast computation: Algorithm of offline recovery involves repeated applications of $\Phi\Psi$. A fast computable Φ is desirable for both encoding imaging and decoding recovery.
4) Physically realizable: Φ should be easily implemented by a hardware such as an optical or analog system.

Frequently used measurement matrices Φ are random matrices, random partial orthogonal matrices, and randomlike transforms, because they are incoherent for almost all sparse transforms. How to build optimal and determined measurement matrices satisfying all of the aforementioned properties is still undergoing.

A prototype of a single-pixel digital camera was presented by Baraniuk *et al.* [6], [9] of the Rice University by using 0/1 random binary matrices for Φ. Rather than recording pixels of the scene under view, the compressed-sensing cameras directly sense geometric and structural information by collecting random projections using a digital micromirror array, which requires just one photosensitive sensor instead of millions [9]. This pixel actually is a compressed projection of multipixel information. This means that the compression step has been cut because compression is made by optical imaging itself, which is useful to reduce data acquisition, power, and storage space. Moreover, fewer light detectors are needed in CS cameras, which saves the cost of expensive detectors. It can also work much more easily for low light and outside the visible light spectrum, so that it is potential for night-vision and infrared imaging. The single-pixel camera is basically an optical computer comprising two lenses, a single photon detector, an analog-to-digital converter, and a digital micromirror device (DMD). A primary optical scheme of the single-pixel camera can be found in [9].

As mathematical interpretation, we first reshape the 2-D image into a 1-D signal $x = \{x_1, \ldots, x_i, \ldots, x_N\}$ and assemble the 2-D Φ matrix using random vector $\Phi_m = \{\Phi_{m,1}, \ldots, \Phi_{m,i}, \ldots, \Phi_{m,N}\}$ $(m = 1, \ldots, K)$ in each row. The random Φ_m is steered by orienting the bacterium-sized mirrors in DMD. The reflecting light field is focused on the single photodiode by lens in order to get one measurement $y_m = \sum_{i=1}^{N} \Phi_{m,i} x_i$. Repeat K times using different Φ_m to obtain all measurements $y = \Phi x$. Such a repetitive operation can be finished in a momentary time by tuning the directions of mirrors in DMD. The camera is single-pixel but multitime (SPMT) imaging. The SPMT camera carries out a sequential imaging which is slower than a parallel imaging of a classical charged coupled device (CCD) camera. However, the SPMT does not need an additional compression step that is required by classical imaging.

The random matrix used in the Rice's single-pixel cameras is universal for general signals, but it is not optimal for a certain case. In this letter, we apply a so-called 2-D noiselet transform [10], [12] as a measurement matrix in the single-pixel cameras. The attractiveness of noiselets is twofold: a fast transform with $\mathcal{O}(N)$ computational complexity is available, which can provide low computational cost; it provides near-optimal measurements for most astronomical data, which can lead less numbers of necessary measurement for a high-quality recovery [10].

We can also consider random Fourier measurement in Φ [11] for different applications, e.g., magnetic resonance imaging in medical engineering and spatially modulated imaging Fourier transform spectrometer in remote sensing. In this case, we obtain the K measurements at the same time by using a random mask on Fourier coefficients of x. This camera carries out a multipixel but single-time (MPST) imaging in Fourier space. The physical prototype of MPST cameras can be implemented easily by an optical system, where the random projections can be implemented within a single exposure by using a random phase mask that is placed on a lens. Alternatively, some prototypes for measurement matrix have also been proposed [13]–[15]. Neifeld and Ke [13] compared three optical

architectures for compressed imaging: sequential, parallel, and photon sharing. Each of these architectures is analyzed using two different types of projection: principal component projections and pseudorandom projections. The performance of each architecture-projection combination is quantified in terms of reconstructed image quality as a function of measurement noise strength. Other interesting possibilities of the measurement matrices are available for future work by using, e.g., Toeplitz block matrices [16] and structurally random matrices [17].

We emphasize that the main contribution of this letter is to introduce a new sensing mechanism for remote sensing, instead of a new compression scheme. With regard to the CS-based lossy compression in comparison with JPEG 2000 format, we refer readers to the study of Goyal *et al.* [18]. We proposed two possible systems including SPMT and MPST for different applications in remote sensing. The physical significant differences between these two encoding approaches are obvious. The SPMT uses a single sensor with a sequential space-domain imaging, while MPST uses multiple sensors (but the number of sensors is still much fewer than those used in traditional CCD cameras) with a parallel Fourier-domain imaging. They have respective pros and cons. The SPMT uses far fewer sensors but has to pay a longer imaging time, while the MPST uses more sensors but saves imaging time. The fewer photon sensors would lead to cameras with smaller size, more portable weight, simpler complexity, and cheaper expense. On the other hand, the decoding of the SPMT needs more computation cost and memory than the MPST, which will be addressed in the next section. Therefore, we say that the compressed-sensing cameras offer a flexible mechanism to take a tradeoff between the space and time according to practical requirements.

III. Offline Decoding: Iterative Curvelet Thresholding

To recover x in (1), the number of nonzero entries and their locations and amplitudes are all completely unknown *a priori*. The *a priori* knowledge that we can use is the sparsity of x. A few recovery algorithms of the CS have been recently proposed. They are based on, e.g., linear programming [1], gradient projection sparse reconstruction [20], orthogonal matching pursuit [19], and iterative thresholding [10], [21], [22]. In this letter, we apply an iterative curvelet thresholding for the decoding of CS.

Curvelet transform [7], [8] is a new geometric multiscale transform. It can be interpreted as an anisotropic geometric wavelet transform, which allows an optimal sparse representation of objects with smooth-curve singularities. Unlike wavelets, the system of curvelets is indexed by three parameters: a scale 2^{-j}, $j \in \mathbb{N}_0$; an equispaced sequence of rotation angles $\theta_{j,l} = 2\pi l \cdot 2^{-\lfloor j/2 \rfloor}$, $0 \le l \le 2^{\lfloor j/2 \rfloor} - 1$; and a position $x_k^{(j,l)} = R_{\theta_{j,l}}^{-1}(k_1 2^{-j}, k_2 2^{-\lfloor j/2 \rfloor})^{\mathrm{T}}$, $(k_1, k_2) \in \mathbb{Z}^2$, where $R_{\theta_{j,l}}$ denotes the rotation matrix with angle $\theta_{j,l}$. The curvelets are defined by

$$\psi_{j,l,k}(x) := \psi_j\left(R_{\theta_{j,l}}\left(x - x_k^{(j,l)}\right)\right) \quad x = (x_1, x_2) \in \mathbb{R}^2.$$

Let $\mu = (j, l, k)$ be the collection of the triple index. The curvelet coefficients are given by $c_\mu(f) := \langle f, \psi_\mu \rangle$. The forward and inverse curvelet transforms have the same computational cost of $\mathcal{O}(N^2 \log N)$ for an $N \times N$ image [8]. The motivation to use the curvelet transform for CS is that most natural scenes consisting of line-singularity edges are very sparse in curvelet domain.

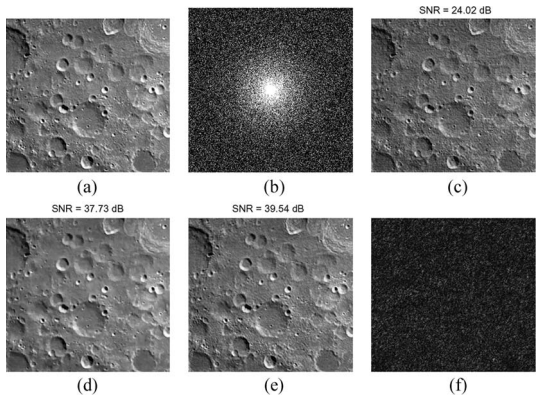

Fig. 1. Compressed remote sensing using MPST with 25% measurements for lunar probe. (a) Original scene of moon's surface. (b) Random sampling scheme. (c) Decode result by zero-filling reconstruction (SNR $= 24.02$). (d) Decode result by wavelets and total variation regularization (SNR $= 37.73$). (e) Decode by iterative curvelet thresholding (SNR $= 39.54$). (f) Decoded error by the curvelet method.

Define a thresholding transform function

$$S_\tau(f, \Psi) = \sum_\mu \tau\left(c_\mu(f)\right) \psi_\mu \tag{3}$$

where τ can be taken as, e.g., a hard thresholding function defined by a threshold $\sigma > 0$, $\tau(x) = x$ if $|x| \ge \sigma$ and $\tau(x) = 0$ if $|x| < \sigma$. We have the iterative curvelet thresholding

$$x_{p+1} = S_\tau\left(x_p + \Phi^{\mathrm{T}}(y - \Phi x_p), \Psi\right) \tag{4}$$

where p denotes the index of iterations. The initial value x_0 can be set to zeros or a zero-filling reconstruction of initial incomplete observation [11]. The highly approximate x can be recovered by stoping the iteration once a given criterion, e.g., $\|x_{p+1} - x_p\| < \varepsilon$, is satisfied. We refer to [7], [8], [23], and [24] for details of the used second-generation curvelet transform and [21] for mathematical properties of iterative thresholding methods.

The decoding is carried out by ground digital computers that undertake most of computational complexity. In terms of the decoding in (4), the MPST camera is faster than SPMT camera because the measurement matrices Φ in MPST have much smaller dimensions than those in SPMT. Mathematically, the computational complexity of MPST is $\mathcal{O}(2P(1+N)N \log N) = \mathcal{O}(2PN \log N + 2PN^2 \log N)$ for an $N \times N$ scene, while those of SPMT is $\mathcal{O}(2PKN^2 + 2PN^2 \log N)$ where $\log N \le K \le N^2$ and P denotes the total number of iterations.

IV. Numerical Experiments

Chang'e-1 lunar probe, China's first circumlunar satellite, blasted off on October 24, 2007. One of scientific objectives of Chang'e-1 is to capture 3-D survey of the moon's surface. In spite of the stereo design, the currently used CCD camera in Chang'e-1 includes a wide-angle lens and 1024 $\times$ 1024 array sensors. Fig. 1(a) shows a picture of moon's surface with resolution of 120 m, captured by the Chang'e-1 at the height of 200 km. We first consider the MPST camera only using 25% measurements for the lunar probe. Fig. 1(b) shows the random sampling point in the Fourier domain. Fig. 1(c)

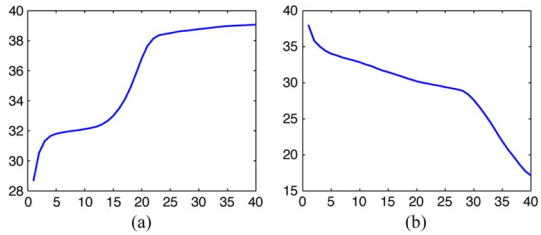

Fig. 2. (a) SNR versus number of iterations. (b) Recovery error versus number of iterations. The horizontal coordinate denotes the number of iterations.

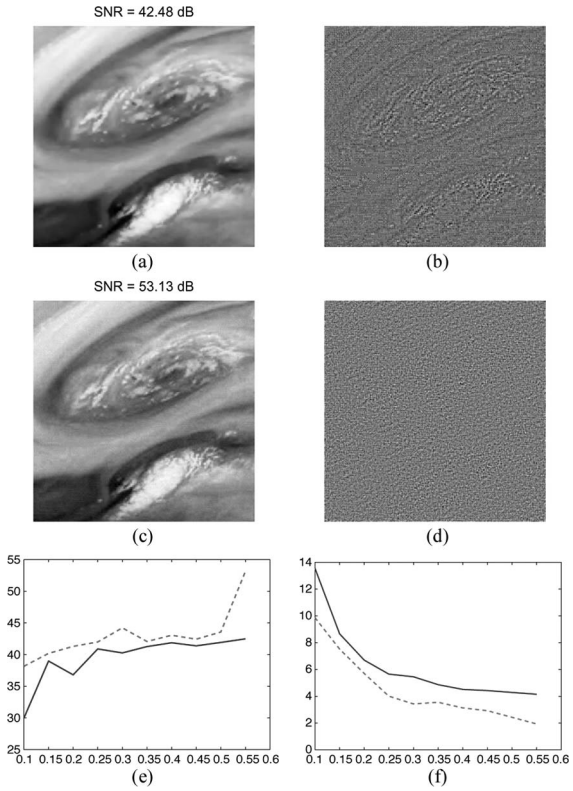

Fig. 3. MPST imaging for a cloud system. (a) and (b) Wavelet decoding and its error. (c) and (d) Curvelet decoding and its error. (e) and (f) SNR and recovery error versus number of measurements by the curvelet decoding. The horizontal coordinate denotes the RMN to total numbers. Dashed lines denote iterative curvelet thresholding, and solid lines denote iterative wavelet thresholding.

shows a decoding result using direct zero-filling reconstruction [11]. Fig. 1(d) shows a decoding result by a proposed method in [11], which solves a convex optimal problem with wavelet transform and total variation constraints by nonlinear gradient projection. Fig. 1(e) shows a result by the proposed iterative curvelet thresholding. A decaying thresholding value $\sigma = \sigma_0(1 - k/K_{\text{iter}})$ is used, where the initial thresholding value $\sigma_0 = 0.06$, k is an index of iterations, and the number of total iterations $K_{\text{iter}} = 40$. The curvelet method recovers edges well and achieves a higher signal-to-noise ratio (SNR) value than other methods. Fig. 1(f) is decoding error by the curvelet method, which basically displays a random noise. The CS camera carries out the compression and denoising at the same time. Fig. 2 shows the change of SNR and recovery error as the number of iterations increases by the curvelet method.

Fig. 3 shows performances of the proposed method for another real remote sensing data with vortex structures. Fig. 3(a) shows a decoding result by an iterative wavelet thresholding

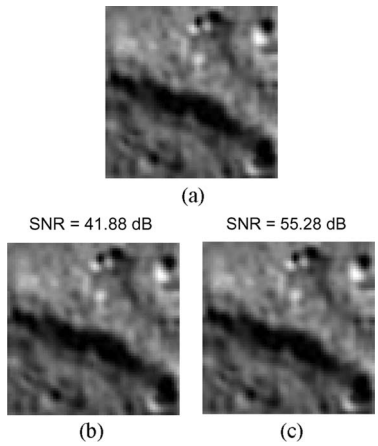

Fig. 4. SPMT imaging for moon's surface. (a) Original unknown scene. (b) Random measurement encoding and curvelet decoding. (c) Noiselet measurement encoding and curvelet decoding.

[i.e., using DB4 wavelets instead of curvelets in (4)], considering 55% measurements. Fig. 3(b) shows the removed components (decoding error) by the wavelet method. Fig. 3(c) and (d) shows the decoding result and error by the iterative curvelet thresholding. Fig. 3(e) shows the change of SNR of decoding results by the two iterative methods, as the number of measurements increases from 10% to 55%. It can be seen that 15% measurements can result in a satisfying result for this case. Fig. 3(f) shows the corresponding recovery errors as the number of measurements increases. The dashed line denotes for the curvelet method, and solid line denotes for the wavelet method. It can be seen obviously that the curvelet method owns high-quality decoding results preserving structural edges well.

We next apply the SPMT cameras for remote sensing. Fig. 4(a) shows an original unknown scene with size 64×64. We first consider random binary measurement matrix in encoding step, which is also used in Rice's single-pixel cameras. Fig. 4(b) shows a result when we apply a random measurement matrix and the iterative curvelet thresholding recovery with 55% measurements and 60 iterations. Fig. 4(c) shows the result when we apply the noiselet transform in the encoding step. The same decoding method and computational parameters have been used in Fig. 4(b) and (c). In order to see clearly the differences between the two encoding approaches, we show the change of SNR and recovery errors as the number of iterations increases in Fig. 5(a)–(d). It can be seen that the noiselet-based imaging method achieves a higher SNR value. Moreover, it has a faster decay in terms of the recovery errors. Fig. 5(e) and (f) shows the change of SNR as the number of measurements increases. Generally, 25% measurements are enough to get a high-resolution result for engineering requirements. Fewer measurements would lead to less storage and less decoding time. From the experiments, the noiselet-based measurements are better than random matrix measurements to some extent. However, for a measurement number smaller than 20%, the noiselet matrix almost fails while the random matrix can obtain an approximate result.

We remarked that the ratio of measurement numbers (RMN) is different from the CR that we used in data compression. Generally, the CR is produced by three steps: sparse transform, quantification of coefficients, and entropy coding, for lossy compression [18]. However, the RMN means the necessary numbers

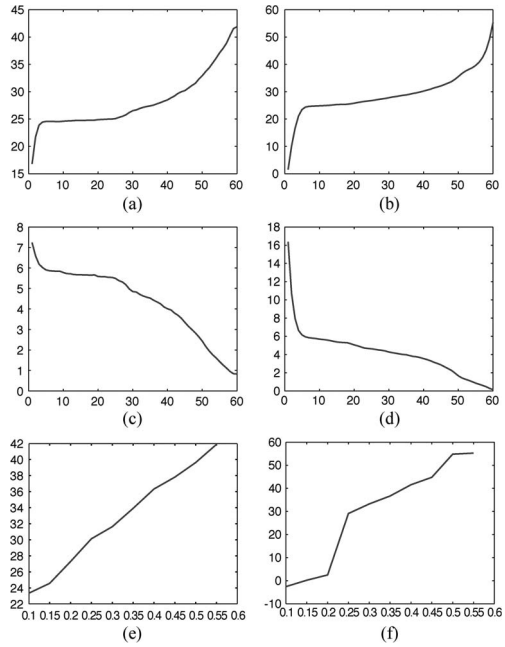

Fig. 5. Comparison of the SPMT imaging with different encoding approaches. (Left column) Random measurement. (Right column) Noiselet measurement. (a) and (b) SNR versus iterations. (c) and (d) Recovery error versus iterations. (e) and (f) SNR versus number of measurements.

to ensure exact (noiseless cases) or highly accurate (noise cases) reconstruction of original unknown signals. The RMN is somewhat like a CR that only uses a random transform step.

Finally, we emphasize that the 2-D noiselet (or random) measurement matrix and random Fourier measurement matrix are applied only to SPMT and MPST, respectively, in this letter. We also remark that we do not pay attention to performance comparisons between SPMT and MPST encoding approaches in this letter but indicate their respective imaging applications.

V. Conclusion

In this letter, we applied a theory of CS for aerospace remote sensing in order to reduce the cost of data acquisition. The CS provides a new sensing mechanism where high-resolution qualities are not directly related to the number of pixels as before but are related to the sparsity or compressibility of signals. The compression is implemented by optical imaging itself without the use of additional compression algorithms. Further applications on deblurring of the CS-based remote sensing can be found in [25]. For video imaging, the CS cameras need no shutter because one merely measures continuously a sequence through randomized Φ_m and then reconstructs a video sequence using a recovery algorithm [9].

Applications of the CS on remote sensing are in their infancy. A huge computer memory is required by the use of current SPMT decoding, particularly for large-scale remote sensing. How to optimally construct the measurement matrices and corresponding fast recovery methods for practical applications is our next work. Currently, all experiments were implemented by computer simulations only. Therefore, another challenging work is to build a physically realizable hardware optical scheme for the CS remote sensing, particularly for stereo CS imaging by exploring a joint sparsity. There is a big room for future research.

Acknowledgment

The author would like to thank the associate editor and the referees for their constructive suggestions, which substantially improved this letter.

References

[1] E. Candès and T. Tao, "Decoding by linear programming," *IEEE Trans. Inf. Theory*, vol. 51, no. 12, pp. 4203–4215, Dec. 2005.
[2] E. Candès, J. Romberg, and T. Tao, "Stable signal recovery from incomplete and inaccurate measurements," *Commun. Pure Appl. Math.*, vol. 59, no. 8, pp. 1207–1223, Aug. 2006.
[3] E. Candès, J. Romberg, and T. Tao, "Robust uncertainty principles: Exact signal reconstruction from highly incomplete frequency information," *IEEE Trans. Inf. Theory*, vol. 52, no. 2, pp. 489–509, Feb. 2006.
[4] D. Donoho, "Compressed sensing," *IEEE Trans. Inf. Theory*, vol. 52, no. 4, pp. 1289–1306, Apr. 2006.
[5] E. Candès and M. Wakin, "An introduction to compressive sampling," *IEEE Signal Process. Mag.*, vol. 25, no. 2, pp. 21–30, Mar. 2008.
[6] R. Baraniuk, "Compressive sensing [lecture notes]," *IEEE Signal Process. Mag.*, vol. 24, no. 4, pp. 118–121, Jul. 2007.
[7] E. Candès and D. Donoho, "New tight frames of curvelets and optimal representations of objects with piecewise C^2 singularities," *Commun. Pure Appl. Math.*, vol. 57, no. 2, pp. 219–266, Feb. 2004.
[8] E. Candès, L. Demanet, D. Donoho, and L. Ying, "Fast discrete curvelet transforms," *Multiscale Model. Simul.*, vol. 5, no. 3, pp. 861–899, Jan. 2006.
[9] M. Duarte, M. Davenport, D. Takhar, J. Laska, T. Sun, K. Kelly, and R. Baraniuk, "Single-pixel imaging via compressive sampling," *IEEE Signal Process. Mag.*, vol. 25, no. 2, pp. 83–91, Mar. 2008.
[10] J. Bobin, J. Starck, and R. Ottensamer, "Compressed Sensing in Astronomy," *IEEE J. Sel. Topics Signal Process.*, vol. 2, no. 5, pp. 718–726, Oct. 2008.
[11] M. Lustig, D. Donoho, and J. Pauly, "Sparse MRI: The application of compressed sensing for rapid MR imaging," *Magn. Reson. Med.*, vol. 58, no. 6, pp. 1182–1195, Dec. 2007.
[12] R. Coifman, F. Geshwind, and Y. Meyer, "Noiselets," *Appl. Comput. Harmon. Anal.*, vol. 10, no. 1, pp. 27–44, Jan. 2001.
[13] M. Neifeld and J. Ke, "Optical architectures for compressive imaging," *Appl. Opt.*, vol. 46, no. 22, pp. 5293–5303, Aug. 2007.
[14] N. Pitsianis, D. Brady, A. Portnoy *et al.*, "Compressive imaging sensors," *Proc. SPIE*, vol. 6232, pp. 623 20A:1–623 20A:9, 2006.
[15] A. Stern and B. Javidi, "Random projections imaging with extended space-bandwidth product," *J. Display Technol.*, vol. 3, no. 3, pp. 315–320, Sep. 2007.
[16] F. Sebert, L. Ying, and Y. Zou, "Toeplitz block matrices in compressed sensing and their applications in imaging," in *Proc. ITAB*, May 30–31, 2008, pp. 47–50.
[17] T. Do, T. Tran, and L. Gan, "Fast compressive sampling with structurally random matrices," in *Proc. ICASSP*, Mar. 31–Apr. 4, 2008, pp. 3369–3372.
[18] V. Goyal, A. Fletcher, and S. Rangan, "Compressive sampling and lossy compression," *IEEE Signal Process. Mag.*, vol. 25, no. 2, pp. 48–56, Mar. 2008.
[19] J. Tropp and A. Gilbert, "Signal recovery from random measurements via orthogonal matching pursuit," *IEEE Trans. Inf. Theory*, vol. 53, no. 12, pp. 4655–4666, Dec. 2007.
[20] M. Figueiredo, R. Nowak, and S. Wright, "Gradient projection for sparse reconstruction: Application to compressed sensing and other inverse problems," *IEEE J. Sel. Topics Signal Process.*, vol. 1, no. 4, pp. 586–597, Dec. 2007.
[21] I. Daubechies, M. Defrise, and C. De Mol, "An iterative thresholding algorithm for linear inverse problems with a sparsity constraint," *Commun. Pure Appl. Math.*, vol. 57, no. 11, pp. 1413–1457, Nov. 2004.
[22] G. Peyré, "Best basis compressed sensing," in *Proc. SSVM*, Jun. 2007, pp. 80–91.
[23] J. Ma and G. Plonka, "Combined curvelet shrinkage and nonlinear anisotropic diffusion," *IEEE Trans. Image Process.*, vol. 16, no. 9, pp. 2198–2206, Sep. 2007.
[24] J. Ma, A. Antoniadis, and F.-X. Le Dimet, "Curvelet-based snake for multiscale detection and tracking of geophysical fluids," *IEEE Trans. Geosci. Remote Sens.*, vol. 44, no. 12, pp. 3626–3638, Dec. 2006.
[25] J. Ma and F.-X. Le Dimet, "Deblurring from highly incomplete measurements for remote sensing," *IEEE Trans. Geosci. Remote Sens.*, to appear, 2009.